

## Atomic contributions to ZnO mechanical properties at negative and positive pressures

Housseem Lakehal<sup>a,b</sup>, Hocine Chorfi<sup>c</sup>, Bachir Zouchoune<sup>a,b</sup>, Álvaro Lobato<sup>d</sup>, Ruth Franco<sup>e</sup>, Pilar Perterra<sup>e</sup>, Miguel Á. Salvadó<sup>e</sup>, J. Manuel Recio<sup>e,\*</sup>

<sup>a</sup> Laboratoire de Chimie appliquée et Technologie des Matériaux, Université Larbi Ben M'Hidi, Oum El Bouaghi, 04000, Algeria

<sup>b</sup> Unité, de Recherche de Chimie de l'Environnement et Moléculaire Structurale, University of Constantine (Mentouri), Constantine, 25000, Algeria

<sup>c</sup> Physics Department, University of Constantine 1, Constantine, 25017, Algeria

<sup>d</sup> MALTA-Consolider Team and Departamento de Química Física, Universidad Complutense de Madrid, Madrid, 28040, Spain

<sup>e</sup> MALTA-Consolider Team and Departamento de Química Física y Analítica, Universidad de Oviedo, Oviedo, 33006, Spain

### ARTICLE INFO

#### Keywords:

First-principles calculations

Equation of state

Negative pressure

Polymorphism

Zinc oxide

### ABSTRACT

The energy-volume curve of a crystalline solid is critically examined in terms of the mechanical contributions of its constituent atoms. In addition to the usual analysis in the positive compression regime, our computational approach covers the tensile behavior in the negative pressure region up to the spinodal stability limit. Using the rich polymorphism of ZnO as a test-bed example, we propose two atomic decomposition schemes that are able to recover the bulk moduli and the critical strengths of four ZnO phases providing an intriguing interpretation of the chemical bonding network as a parallel circuit of mechanical resistors. Our scheme also allows the identification of the role played by the cation and anion in the densification of the high-pressure polymorphs and up to the material rupture points. This approach may help in the quest for tailored materials with outstanding mechanical performance.

### Introduction

In a crystalline solid, the calculated electronic energy ( $E$ )-volume ( $V$ ) curve represents its equation of state (EOS) at static conditions, i.e., at 0 K and zero point vibrational contributions neglected. This computational approach is very reasonable in describing hydrostatic pressure ( $p$ ) effects on a variety of non-molecular solids at least up to room temperature since in this class of materials thermal expansion coefficients are as low as  $10^{-5}$ – $10^{-6}$  K<sup>-1</sup>. Thanks to the combination of the static approximation with accurate first-principles computational methodologies, databases containing calculated EOS parameters are now often used in machine learning protocols to help the engineering of materials with specific properties [1–4]. In opposition to this ongoing strategy, studies directed to the in-depth understanding of specific values and the trends of these EOS parameters in terms of the atomic constituents of the crystalline solids are much less frequent and constitute a necessary perspective complementary to brute force schemes.

Whereas most of the efforts have been directed toward the exploitation of the  $E$ - $V$  curve in the region with  $V$  values lower than the equilibrium volume ( $V_0$ ), negative pressures appearing at  $V > V_0$  have been scarcely explored so far (see for example [5–8]). The main reason is probably the experimental difficulty in expanding isotropically a

solid. However, this fact has not hindered the observation of negative pressure states in materials [9,10]. Epitaxial [11] and nanoparticle growth [12], chemical substitution, or ion extraction [13] induce crystal elongations, which can be understood if we assume that negative pressures are present.

Computational experiments exploring the tensile “hydrostatic” expansion of a given material are needed in this regard and also yield valuable information about strain-induced phenomena such as the stability limit (spinodal point) and the ideal strength of materials under tensile conditions [14]. For instance, a modified spinodal EOS has been recently proposed to evaluate the rupture conditions of a collection of prototypical layered crystals subjected to uniaxial and biaxial negative stresses [15]. The importance of these properties in the materials science field makes it necessary to develop equations of states and atomic models directed to analyze materials under “hydrostatic” tensile conditions.

In this study, we employ a computational strategy based on partitioning the crystalline space into atomic basins using Bader’s topological analysis [16]. Similar to the Crystal Chemistry formalism, which identifies and transfers polyhedral functional-like groups between different compounds [17–20], this approach facilitates the decomposition of observable properties (e.g., volume, bulk modulus, ideal

\* Corresponding author.

E-mail address: [jmrecio@uniovi.es](mailto:jmrecio@uniovi.es) (J.M. Recio).

strength) into local contributions associated with different chemical elements [21]. Furthermore, we introduce an intriguing analogy between the crystalline bonding network and a parallel circuit of mechanical resistors [22]. This analogy becomes apparent when we focus on the energy cost associated with the volume reduction or expansion of each atomic constituent from its equilibrium value.

We have selected wurtzite, zincblende, rock-salt, and cesium chloride ZnO polymorphs to illustrate the bonding network-mechanical circuit analogy and to evaluate how the changes in the atomic mechanical properties of Zn and O along with the polymorphic sequence affect their observable EOS parameters. ZnO shows a well-known pressure-induced polymorphism with experimental data at tensile conditions too, thus providing a simple yet realistic case study to calibrate the performance of our approach. This is an important fact that has motivated us to select ZnO as the test-bed material to undergo our microscopic partition analysis at both positive and negative pressure regimes. ZnO is also a genuine prototype of a binary crystal with similar atomic sizes (BCSAS) despite presenting ionic radii with differences as large as 0.6 Å (Zn<sup>2+</sup>) and 1.4 Å (O<sup>2-</sup>). Based on these ionic sizes, we could expect different atomic mechanical responses under pressure. This fact constitutes a challenge in the study of local mechanical properties and has also other implications related to nucleation and growth processes of phase transitions.

The main aim of the study is to provide insights into the atomic mechanism by means of which a given ZnO phase reduces or expands its volume at positive and negative pressure, respectively. To achieve this goal, we have exploited the information enclosed in the whole  $E$ - $V$  curves of the four ZnO phases by applying two different atomic decomposition schemes. As a result, several mechanical properties, such as the zero pressure bulk modulus and the critical strength, have been split into Zn and O contributions. In all cases, we pursue to show that our chemical protocol is useful to understand particular, mainly mechanical, structure–property relationships of a given polymorph.

### Computational details of electronic structure calculations and equation of state fittings

First-principles electronic structure calculations and geometry optimizations of polytype structures of ZnO are carried out under the Kohn–Sham DFT framework with the ABINIT code [23] using the Perdew–Burke–Ernzerhof (PBE) exchange–correlation functional [24]. The so-called FHI atomic plane wave pseudopotentials [25] are adopted, while cutoff energies and Monkhorst–Pack grids [26] are set to 600 eV and  $8 \times 8 \times 8$  and  $8 \times 8 \times 6$  for cubic- and hexagonal-ZnO, respectively. Atomic positions are optimized until the total energy converges within 0.1 meV. At the same time, all crystalline strains were optimized so that the corresponding stress components turned out to be within 100 MPa from a predetermined value. The Broyden–Fletcher–Goldfarb–Shanno minimization scheme (BFGS) [27] was used. In this way, stress-volume curves under controlled hydrostatic stress were obtained. Critical strength (ideal strength) was determined as the maximum value of hydrostatic stress before the lattice loses stability and the forces diverge. Atomic positions and movements through the different paths are analyzed using VESTA, a visualization program for structural models [28].

Our computational strategy consists of electronic energy calculations for each polymorph within a volume interval expanding lower and higher volumes than the equilibrium one. All extensive magnitudes in our study are per formula unit. For each set of  $(E_i, V_i)$  calculated data, we perform the equation of state fittings using our GIBBS2 code [29,30]. Integrated analytical  $E(V)$ , pressure  $(p)$ - $V$ , and enthalpy  $(H)$ - $p$  curves are rigorously determined for all the polymorphs, and their stability pressure regions evaluated by applying the equilibrium condition at the static approximation ( $\Delta H = 0$ ), where  $\Delta$  refers to the difference of enthalpies between two phases.

By means of the topological partition carried out using Bader’s Atoms in Molecules formalism [16,31], the unit cell volumes per formula unit ( $V$ ) of the B1, B2, B3, and B4 ZnO polymorphs are decomposed into disjoint atomic contributions ( $V_{\text{Zn}}, V_{\text{O}}$ ) that fill up the whole space:  $V = V_{\text{Zn}} + V_{\text{O}}$ . These atomic basins are defined by surfaces where the flux of the electron density gradient is zero. Each atomic basin contains either the nucleus of Zn or O and encloses a volume that is evaluated using the bisection method with a Gauss–Legendre quadrature as implemented in the Critic2 code [31]. Standard options were selected for other computational parameters. In this way, we have evaluated the volumes of Zn and O at different pressures for each polymorph and evaluated the fractional occupation of the two atoms by dividing these volumes with respect to the corresponding volume of the formula unit at zero pressure for each polymorph. This procedure allows us to determine  $(p_i, V_i)$  data for Zn and O, and the corresponding atomic EOS in all the ZnO polymorphs.

### Local decomposition schemes

We propose two decomposition schemes that look for physical-chemical insight into the atomic-level mechanism followed by a given material to increase its density under hydrostatic pressure. If we know which particular chemical constituent of the solid is the one with the lowest compressibility (among a potential set of components), then we can anticipate and guide the synthesis of materials with desired elastic properties. To get reliable information about this mechanism, an exhaustive partition of the unit cell space in terms of meaningful chemical entities is required. This feature is achieved by the two decomposition schemes applied in this work using the well-known Quantum Theory of Atoms in Molecules formalism developed by Richard Bader and co-workers [16].

The advantage of the standard atomic partition is the capability of providing equations of state (EOS) of the chemical elements belonging to the solid mimicking the crystalline EOS. The possibility of atomic EOS transference between different materials is also another advantage of this partition. In the second scheme, as the emphasis is on the total energy of the solid, the partition provides an intuitive interpretation on how the mechanical properties of the solid are distributed among the atomic components following an electrical–mechanical analogy. Moreover, this second scheme, allows us to monitor the energy storage upon pressure application in terms of the atomic constituents.

Regarding limitations, both schemes are of general application provided the solution of the Schrodinger solution of a periodic crystalline solid is known. This means that the limitations are those inherent to the methodologies used in first-principles solid state calculations, *i.e.* disordered and amorphous solids or crystals with unit cells containing a very large number of atoms would be prohibitive for analysis with these two schemes.

### Standard atomic EOS partition

Using a formally equivalent definition as for the macroscopic system, local atomic compressibilities ( $k_i$ ) at zero pressure can be expressed as follows Martín Pendás et al. [21]:

$$k_i = -\frac{1}{V_i} \frac{\partial V_i}{\partial p} \quad (1)$$

An expression for the zero pressure bulk compressibility ( $k_0$ ) of any crystalline polymorph can be straightforwardly derived in terms of atomic contributions:

$$k_0 = \sum_i f_i k_i; \quad f_i = \frac{V_i}{V_0} \quad (2)$$

where  $f_i$  is the fractional occupation of the  $i$ th atomic constituent of the solid in the unit cell, whose volume per formula unit is  $V_0$  at zero pressure. The atomic contributions to the zero pressure bulk modulus ( $B_0$ ) are implicitly contained in this expression since  $B_0 = \frac{1}{k_0}$  [19,21].

The only requisite for these equations to be valid is that the unit cell volume is filled out with non-overlapping atomic volumes:  $V = \sum_i V_i$ . We say that this unit cell partition is exhaustive. This partitioning has been widely applied to explain for example how the compressibility of spinels is determined mainly by the anion sublattice [32], the bonding reconstruction across solid–solid phase transitions [33,34], optical properties in ceramics [35], or the pressure behavior of several carbonates at mantle conditions [20].

When the above equations are applied to any of the ZnO polymorphs, the decomposition is as simple as

$$k_0(\text{ZnO}) = f_{\text{Zn}} k_{\text{Zn}} + f_{\text{O}} k_{\text{O}}. \quad (3)$$

$k_0(\text{ZnO})$  can be easily evaluated with this expression once the atomic volumes  $V_i$  and the  $p$ – $V$  curve are obtained from the calculated  $E$ – $V$  curve of a given ZnO polymorph. Thus,  $B_0(\text{ZnO}) = 1/k_0(\text{ZnO})$  can be recovered and compared with the value from the  $E$ – $V$  fitting.

### Local pressures as resistors of a parallel mechanical circuit

A less conventional atomic partition proposed by Ouahrani et al. [22] is also worth to be applied to analyze the mechanical properties at positive and negative pressures. Let us consider the thermodynamic definition of pressure at the athermal limit  $p = -\frac{\partial E}{\partial V}$ . This definition involves increasing of the crystal energy out of its equilibrium volume. It also follows from this definition (using absolute values) that pressure is a measure of the mechanical resistance of the solid to change its volume. A decomposition of this resistance in terms of Zn and O constituents of ZnO polymorphs is obtained by using a similar definition for the local pressures  $p_{\text{Zn}}$  and  $p_{\text{O}}$  as follows:

$$p_{\text{Zn}} = -\frac{\partial E}{\partial V_{\text{Zn}}}, \quad p_{\text{O}} = -\frac{\partial E}{\partial V_{\text{O}}}. \quad (4)$$

Just considering that  $V = V_{\text{Zn}} + V_{\text{O}}$ , it is easy to show that the total mechanical resistance or pressure behaves analogously as the resultant resistance of an electronic circuit of parallel resistors [22]:

$$\frac{1}{p} = \frac{1}{p_{\text{Zn}}} + \frac{1}{p_{\text{O}}}. \quad (5)$$

This partition allows us to interpret the material's mechanical resistance as due to the contribution of the mechanical resistance of its atomic constituents. Similarly to Ohm's Law applied to a circuit of parallel electric resistors, the mechanical energy stored by changing the crystal volume is evaluated using the above equation in which the atoms act as parallel mechanical resistors. To make it more evident, the roles played by the electric voltage, the current intensity, and the electrical resistance in a parallel electrical circuit are in this analogy played by  $\Delta E$ ,  $\Delta V$ , and  $p$ , respectively. In fact,  $\Delta E = \Delta V \times p$ , being  $\Delta V$  the sum of the atomic contributions, in analogy with the total current being the sum of the intensities across the branches of the parallel circuit:

$$\Delta V = \Delta V_{\text{Zn}} + \Delta V_{\text{O}}. \quad (6)$$

In this decomposition scheme, the zero pressure bulk moduli of the atomic constituents (we omit the 0 subscript to simplify the notation) are defined as:

$$B_i^{\text{MR}} = -V \frac{\partial p_i}{\partial V}, \quad (7)$$

where the superscript MR helps to differentiate the atomic  $B_0$  parameter defined in the standard atomic decomposition from the one defined under this ‘‘mechanical resistance’’ (MR) analogy.

Using Eq. (5), the total and local pressure differentials are related as follows:

$$dp = \sum_i \left( \frac{p}{p_i} \right)^2 dp_i, \quad (8)$$

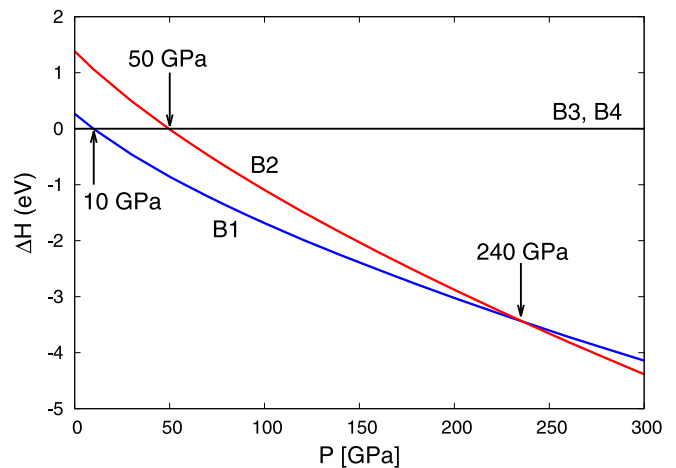


Fig. 1.  $\Delta H$  evolution with pressure for the ZnO polymorphs explored in this work. B3 and B4 differences in enthalpy are within calculation accuracies and have been taken as the zero value reference.

and, therefore, we can recover the crystal zero pressure bulk modulus as:

$$B_0 = -V \sum_i c_i^2 \left( \frac{\partial p_i}{\partial V} \right) = \sum_i c_i^2 B_i^{\text{MR}}, \quad (9)$$

where the  $c_i$  coefficients are the  $\frac{p}{p_i}$  ratios that can be obtained by linear fittings of the  $p_i$ – $p$  plots.

In the case of ZnO polymorphs these expressions become quite simple:

$$B_0 = c_{\text{Zn}}^2 B_{\text{Zn}}^{\text{MR}} + c_{\text{O}}^2 B_{\text{O}}^{\text{MR}}, \quad c_{\text{Zn}} = \frac{p}{p_{\text{Zn}}}, \quad c_{\text{O}} = \frac{p}{p_{\text{O}}}. \quad (10)$$

## Results and discussion

### Positive pressures

#### Macroscopic view

The behavior of ZnO under hydrostatic pressure has been explored both experimental and computationally many times. See for example [36,37]. Besides the two stable polymorphs at zero pressure (B3 and B4), the observation of the rocksalt (B1) structure at pressures from around 9 GPa onwards is well documented [36]. However, this B1 phase has not been retained at ambient conditions when the pressure is released. Likewise, the B2 phase has been theoretically proposed as the stable phase at pressures higher than 119.5 GPa [38] or 250–260 GPa [39] depending on the calculation procedure.

In Fig. 1, we observe that two phase transitions are predicted for ZnO according to our calculations. The first one leads to the rocksalt structure around 10 GPa, and the second one informs of the emergence of the B2 structure at around 240 GPa, in good agreement with Refs. Reio et al. [36], Wang et al. [39], respectively. These results are obtained whether the B3 or B4 phase is chosen as the stable low-pressure phase. We notice that if the B1 phase is skipped due to for example kinetic barriers associated with the B4–B1 or B3–B1 transition, the B2 structure would appear directly from the B4 or B3 phase at pressures around 50 GPa, which does not seem to be highly feasible. As the B3 (cubic zinc blende) and B4 (hexagonal wurtzite) are nearly energy degenerated, and display almost identical  $E$ – $V$  curves, we choose to discuss results only from the more simple B3 structure in what follows.

The zero pressure unit cell volume per formula unit ( $V_0$ ), the inverse of the compressibility at zero pressure ( $B_0$ ), and its pressure derivative also evaluated at zero pressure ( $B'_0$ ) are the three basic fitting parameters describing the volume evolution with the pressure

**Table 1**

Calculated crystal and atomic EOS parameters and occupation fractions in the B4, B3, B1, and B2 polymorphs of ZnO according to our calculations are gathered in the first row of each polymorph. Range of values of crystal properties reported in Desgreniers [40] and Wang et al. [39] are included with labels *a* and *b*, respectively. Volumes in Å<sup>3</sup> and bulk moduli in GPa.

	ZnO			Zn				O			
	$V_0$	$B_0$	$B'_0$	$V_{Zn}$	$B_{Zn}$	$B'_{Zn}$	$f_{Zn}$	$V_O$	$B_O$	$B'_O$	$f_O$
B4	25.41	122.6	5.0	11.54	128.1	5.3	0.454	13.87	116.5	4.6	0.546
<i>a</i>	23.80–24.57	136–183	3.6–9.4								
<i>b</i>	23.59–24.89	129–183	3.6–4.5								
B3	25.40	127.4	4.4	11.40	133.8	4.7	0.449	14.03	126.8	4.3	0.551
<i>b</i>	23.09–24.86	130–168	3.8–4.6								
B1	20.87	163.0	4.5	9.18	169.1	4.6	0.444	11.52	152.2	4.2	0.556
<i>a</i>	18.85–19.80	132–228	3.5–9.5								
<i>b</i>	18.82–20.61	165–230	3.5–4.6								
B2	19.91	158.6	4.5	9.20	158.2	4.5	0.465	10.60	155.1	4.4	0.535
<i>b</i>	17.85–19.55	161–205	4.4–4.7								

of a given polymorph. These EOS parameters for the low- and high-pressure phases of ZnO are collected in the first four columns of Table 1. The unit cell volumes per formula unit ( $V_0$ ) of the B4 and B3 phases show expected similar values due to their short-range equivalent atomic coordination spheres, whereas  $V_0$  is lower for the high pressure phases. Wang et al. [39] have recently gathered several experimental and calculated  $V_0$ ,  $B_0$ , and  $B'_0$  values for the different ZnO polymorphs. Previous data from Desgreniers [40] are also collected in Table 1. Overall, the good agreement between these previously reported data and our EOS parameters supports the calculated  $E-V$  curves. Higher  $V_0$  and lower  $B_0$  values are within the expectations from GGA-PBE calculations. We notice a non-common trend in the values of  $B_0$  along the polymorphic sequence since the increase in its value after the transition from B3 to the B1 phase is followed by a decrease in the B2 phase. Such conduct has been found earlier for the same B1-B2 transition in other simple binary compounds as the alkali halides. Recio et al. [41], Hofmeister [42] This behavior can be explained by taking into account that the compressibility of the high-pressure phase results from the balance between the higher coordination index (more effective packing) in the B2 phase and the simultaneous increase of the Zn–O bond lengths which decreases the bond strength. It seems that this last effect slightly dominates the balance when the B1 ( $B_0 = 163.0$  GPa) and B2 ( $B_0 = 158.6$  GPa) phases are compared in ZnO.

#### Atomic equations of state

As explained in Section “Standard atomic EOS partition”, the calculated atomic volumes at different unit cell volumes constitute the raw data to evaluate the EOS parameters of Zn and O gathered in Table 1. These values allow us to extract information about the main atomic mechanism of compression of ZnO polymorphs. The first point to remark on is the similarity between the volumes and compressibilities of the two atomic constituents of ZnO. Differences between Zn and O atomic  $B_0$  values are always less than 10% in all the polymorphs, and the highest occupation fraction (oxygen in the B1 phase) is lower than 0.560, which means that the size of both constituents are not so different. Although in all the cases the anion is the most compressible species and the one with the highest occupation in the unit cell, zinc oxide is a good example of a crystalline solid in which the effect of pressure on its structure is distributed almost equally between its two atomic constituents. It is secondly noticeable that the occupation fraction of the atoms remains almost unchangeable regardless of the phase. Thirdly, when Eq. (3) is checked using the atomic data of Table 1, the bulk modulus of the corresponding polymorph is recovered within a discrepancy of less than 2.3%. Values obtained from the atomic EOS (in brackets calculated from the crystal  $E-V$  curve) are 121.5 GPa (122.6 GPa), 129.5 GPa (127.4 GPa), 159.3 GPa (163.0 GPa), and 156.5 GPa (158.6 GPa) for B4, B3, B1, and B2, respectively. This is a proof of the consistency of this decomposition scheme and provides validity to our computational approach.

These findings are also present when the phase transitions are examined. For example, the relative reduction of the volume of Zn

(−18.5%) and O (−17.0%) across the B3-B1 transition at 10 GPa is very similar to the volume collapse of ZnO (−17.5%) according to our calculations. The same is obtained for the change in the bulk modulus at the transition pressure: +19.7% (Zn), +14.2% (O), +18.7% (ZnO). The lower value of O than Zn is compensated by a greater occupation factor of the oxygen ( $f_O$ ) in the unit cell (see Eq. (3) and Table 1). Overall, pressure affects Zn and O almost the same (Zn is only slightly more reluctant to reduce its volume) even when a phase transformation occurs.

We can extend the results in ZnO to analyze the response to pressure of polymorphs of other compounds, especially of those binary crystals whose atoms display similar sizes, BCSAS. From the EOS of one of their atomic constituents, EOS parameters of the bulk material can be anticipated (see Table 1). Examples of such crystals in the alkali halide family are KF, RbCl, CsCl, and CsBr, where atomic occupation fractions between 0.4 and 0.6 are found [21]. It is to be pointed out that in these cases, as well as in ZnO, differences in the ionic radii of the two constituents can be meaningful and should not be used to select crystals belonging to this group as the following values reveal:  $R(\text{Zn}^{2+}) = 0.74$  Å,  $R(\text{O}^{2-}) = 1.40$ ;  $R(\text{K}^+) = 1.38$  Å,  $R(\text{F}^-) = 1.33$  Å;  $R(\text{Rb}^+) = 1.52$  Å,  $R(\text{Cl}^-) = 1.81$  Å;  $R(\text{Cs}^+) = 1.67$  Å,  $R(\text{Br}^-) = 1.96$  Å [43]. Ionic sizes derived from ionic radii can be in contrast with the particular atomic volume values of Bader’s partition of the unit cell. The latter is exhaustive, as we have remarked earlier, and the shape of the ions in the unit cell is not spherical, thus leading in these examples to a similar distribution of the unit cell space between the two constituents despite having different ionic radii.

BCSAS crystals also display particular features regarding nucleation and growth processes in pressure-induced phase transitions. As discussed by Zahn and Leoni [44], the preference for small or big nucleation domains depends on the softness and hardness of the constituents and on the atomic size, which has also implications in the final morphology of the polymorphs. If the ionic mismatch is great, many small domains appear in the growth process as opposed to the situation of BCSAS compounds. Thus, the identification of BCSAS compounds, such as ZnO, is a side result of our decomposition scheme that allows us to propose the formation of few and large domains when pressure-induced ZnO phases are formed.

#### Local mechanical resistances

The mechanical resistance of the crystal to reduce its volume is always lower than that of Zn and O. Although this may seem counterintuitive, it is easy to understand if we realize that, according to Eq. (6), the volume reduction is greater in the bulk than in its constituents. In other words, the ZnO crystal offers a lower resistance than Zn and O. In Fig. 2, we also observe that, although blue (Zn) and red (O) curves are all mixed, Zn curves are slightly displaced to lower volumes than O. We have also shown earlier that the occupation fractions of Zn and O are around 0.45 and 0.55, respectively. More difficult to visualize is that, when the unit cell volume decreases, the corresponding decrease in the

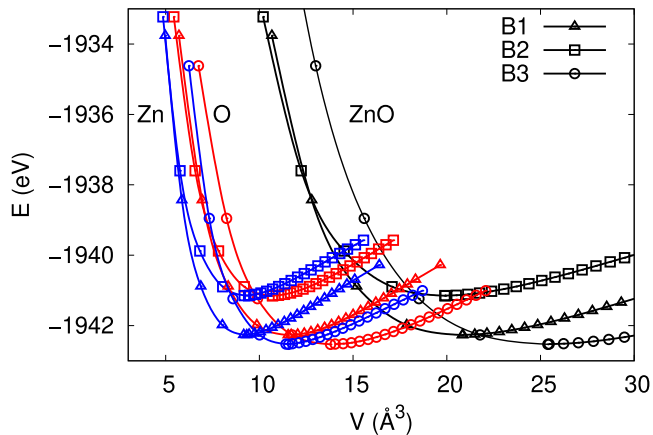


Fig. 2. Calculated  $E-V$  and  $E-V_i$  curves for ZnO (black), Zn (blue), and O (red) for B1, B2, and B3 phases.

Table 2

Fitting coefficients ( $c_i$ ) of the  $p_i-p$  data collected in Fig. 3 and mechanical resistance (MR)-like bulk moduli ( $B_i^{\text{MR}}$ ) in GPa for the B3, B1, and B2 phases of ZnO. Percentual deviations ( $\Delta$ ) in  $B_0$  evaluated with Eq. (10) ( $B_0^{\text{Eq.10}}$ ) with respect to the corresponding ZnO EOS parameters of Table 1 are collected in the last column.

	Zn		O		ZnO	
	$c_{\text{Zn}}$	$B_{\text{Zn}}^{\text{MR}}$	$c_{\text{O}}$	$B_{\text{O}}^{\text{MR}}$	$B_0^{\text{Eq.10}}$	$\Delta$
B3	2.349	271.9	1.732	237.9	128.5	+0.86
B1	2.275	343.9	1.764	305.5	164.5	+0.92
B2	2.117	316.9	1.860	314.3	161.5	+1.83

volume of Zn is also slightly lower than in O. Therefore, the energy stored upon volume compression is achieved as a result of a greater compression of the oxide anions than of the Zn cations. This means that Zn cations, as expected, are more resistant from a mechanical point of view.

The local pressures or atomic mechanical resistances calculated with Eq. (4) are plotted against the total pressure in Fig. 3. Zn and O values in the B3, B1, and B2 phases are all included in this plot. It is remarkable to see that all the points follow two well-differentiated linear trends regardless of the polymorph, one for the cation (slope  $2.23 \pm 0.12$ ) and the other for the anion (slope  $1.79 \pm 0.07$ ). We find a greater slope for Zn (more reluctant to decrease its volume than O), which is consistent with the atomic bulk moduli discussed in the previous subsection. Similar results were obtained in calculations of local pressures in the rest of Zn chalcogenides [22] and in CdTe [45].

Using linear fittings for Zn and O in each polymorph, the coefficients  $c_i$  of Eq. (10) are obtained (see Table 2). Similarly, the bulk moduli of Zn and O under this local mechanical resistance scheme ( $B_i^{\text{MR}}$ ) are also evaluated using the calculated  $p_i$  values and Eq. (7). In this way,  $B_0$  values for the three polymorphs can be recovered. We find again discrepancies only lower than 2% between the values obtained from the  $E-V$  fittings and those evaluated from Eq. (10). This result provides consistency to the different fitting procedures carried out in our study. Moreover, the success in recovering bulk properties from the two decomposition schemes is a relevant result that supports our atom-level approach.

When comparing values of  $B_i$  from Table 1 with those of  $B_i^{\text{MR}}$  in Table 2 differences are apparent. This is not unexpected since the definition used to evaluate the bulk moduli for Zn and O is not the same in the two decomposition schemes. The important point is to see that in both approaches the cation is the one with the highest value in all the polymorphs. Moreover, the difference in the compressibility of Zn and O changes with the polymorph, being greater in B3 and B1 than in B2, but is of the same order regardless of the decomposition scheme.

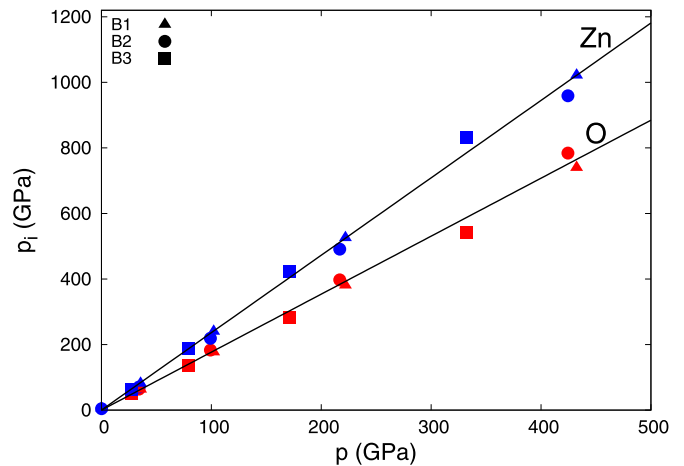


Fig. 3. Calculated  $p_i-p$  curves for Zn (blue), and O (red) for all phases.

An interesting link between our atomic mechanical resistivity and the softness/hardness of the constituents of the crystal can be derived from our results. In our approach, the atomic softness/hardness is controlled by two factors. One is the local bulk moduli  $B_i$ , which can be transferred among different structures. The other are the  $c_i$  coefficients that account for the particular environment of the atom in a given structure. In the case of the BCSAS crystals, these two factors tend to offset each other, resulting in similar mechanical resistances as it happens in ZnO, where  $c_{\text{Zn}}$  is only 1.2 times greater than  $c_{\text{O}}$ . We can speculate that for crystals other than BCSAS, differences in  $p_i$  values would lead to meaningful differences in the hardness value of each constituent. In that case, a different mechanism in the nucleation and growth process would be expected for these materials when experiencing phase transitions.

#### Negative pressures

#### Macroscopic view

In this subsection, we present and discuss the calculated stress-strain curves of the ZnO phases under hypothetical hydrostatic tensile conditions. The strain variable is the relative change in volume from the equilibrium value,  $\epsilon = \frac{V-V_0}{V_0}$ . Remember that in the static approximation  $p = -\frac{\partial E}{\partial V}$ , pressure values in the positive strain regime (here equivalent to stress or tensions) are negative since an increase of volume also implies greater energy. Notice that, usually, in experimental and theoretical tensile works stress is positive.

The relevant parameters at this volume regime of the  $E-V$  curve with positive strains require the second derivative of the energy with respect to volume to be zero. The corresponding volume and pressure in this point are called the spinodal volume,  $V_{\text{sp}}$ , and the spinodal pressure,  $p_{\text{sp}}$ , respectively. Under this condition  $B_0$  is zero, the cohesion forces of the crystal are not able to withstand tensile effects, and the crystal becomes mechanically unstable. Therefore, the spinodal pressure can be understood as the ideal or critical strength ( $\sigma_c$ ) of the crystal, whereas the associated strain is the spinodal volume, which provides the critical strain ( $\epsilon_c$ ) or the greatest strain that the crystal is able to withstand.

The common strategy found in the majority of studies to determine  $\sigma_c$  and  $\epsilon_c$  consists of evaluating the stress tensor at different tensile conditions until a maximum in the stress-strain curve is obtained. In our study, we provide an independent computational procedure to evaluate the critical or ideal strength of polymorphs by applying the spinodal condition to the corresponding energy-volume curves. In Fig. 4, we collect the strain-stress curves of the B3, B1, and B2 phases of ZnO obtained using the Vinet EOS [46] fitted to the calculated  $E-V$

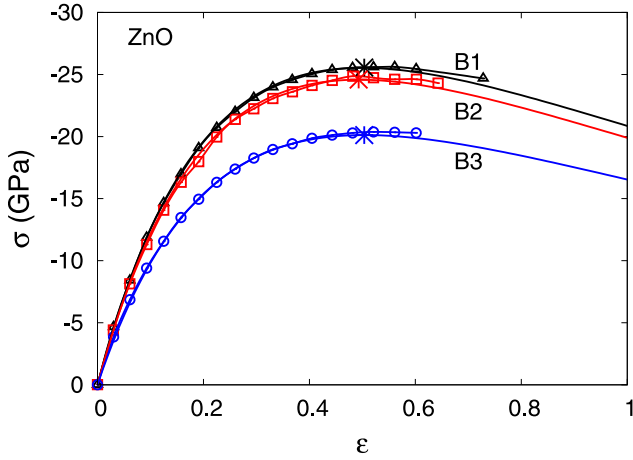


Fig. 4. Calculated stress–strain curves for B3, B1, and B2 phases of ZnO.

points in the negative pressure regime. We have checked that similar results are obtained using other analytical EOS implemented in our GIBBS2 code [29,30]. One advantage of this alternative proposal is that it also allows us to anticipate critical conditions without arriving at the rupture limit.

We can check this advantage by analyzing the calculated ideal or critical stress values:  $-20.1$  GPa (B3),  $-25.6$  GPa (B1), and  $-24.6$  GPa (B2). These  $\sigma_c$  values follow a similar pattern as the one obtained for the bulk moduli of these phases. In particular, the change in the trend after the B1 phase reflects the decrease in the  $B_0$  value discussed in Section “Macroscopic view” when passing from the B1 to the B2 phase. In fact, there is a relationship between spinodal pressures and bulk moduli that connects the compression and tensile behavior of materials and explains this correlation. Generally, this relationship can be written as Brosh et al. [47]:

$$\sigma_c = p_{sp} = -\beta \frac{B_0}{B'_0}, \quad (11)$$

where  $\beta$  is a parameter that depends on the equation of state and can be easily obtained by imposing the spinodal condition. For instance, in the case of the Murnaghan EOS  $\beta = 1$ .

As regards critical strain values, the noticeable feature is that they are all around 0.5 regardless of the phase: 0.504 (B3), 0.503 (B1), and 0.503 (B2). This is consistent with the slopes of the stress–strain curves at the origin that become very similar for the B1 and B2 phases, being lower for B3 in agreement with the corresponding  $B_0$  values. Moreover, the similarity of  $\epsilon_c$  in the three phases also manifests the universality in the shape of the energy–volume curves. Specifically, an analysis of the potential energy curves revealed that rupture distances, or in our case critical strains, are approximately constant regardless the ionic, covalent, or metallic nature of the bonds involved [48]. This universality is manifested in the Vinet EOS [46], where the critical strain can be written as:

$$\epsilon_c = \frac{V_{sp}}{V_0} - 1 = \frac{1}{8X_0^3} (X_0 - 1 + \sqrt{X_0^2 + 6X_0 + 1})^3 - 1, \quad (12)$$

with  $X_0 = \frac{3}{2}(B'_0 - 1)$ . Using a value for  $B'_0$  of 4.5, which is representative of the B1, B2, and B3 phases (see Table 1) and falls within the typical range of values found in the majority of solids. The latter equation yields a critical strain of 0.492, in perfect agreement with our results. A clear conclusion is that our strategy can be used to anticipate the rupture limits (critical stress and strain) of materials under hypothetical hydrostatic tensile conditions, knowing only the bulk modulus and its zero-pressure derivative. This is an extension of the previous study where critical parameters under uniaxial with and without transverse stress were found in good agreement with available data for different covalent compounds [15].

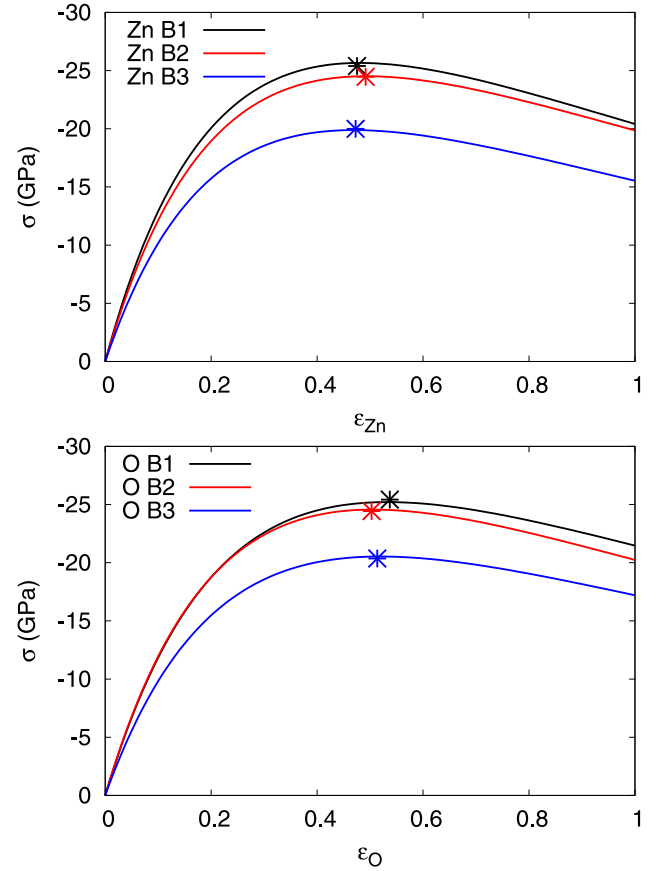


Fig. 5. Calculated stress–strain curves in the B3, B1, and B2 phases of ZnO for Zn (top) and O (bottom).

Table 3  
Spinodal parameters for the bulk, Zn, and O in B3, B1, and B2 phases of ZnO.

	ZnO		Zn		O	
	$p_{sp}^{ZnO}$	$\epsilon_c^{ZnO}$	$p_{sp}^{Zn}$	$\epsilon_c^{Zn}$	$p_{sp}^O$	$\epsilon_c^O$
B3	-20.1	0.504	-20.0	0.473	-20.4	0.514
B1	-25.6	0.503	-25.4	0.476	-25.4	0.486
B2	-24.6	0.488	-24.5	0.492	-24.4	0.503

#### Spinodal parameters from atomic EOS and local mechanical resistances

Our atomic decomposition of EOS parameters also provides information on the rupture mechanism of the crystal under tensile conditions in terms of its constituents. In Fig. 5, we present the atomic stress–strain curves for Zn (top) and O (bottom) in the B3, B1, and B2 polymorphs. A short explanation is needed to indicate how these curves are plotted. In Fig. 4, each negative pressure (stress) value is associated with a unit cell volume that in turn is split into the atomic volumes  $V_{Zn}$  and  $V_O$ . Thus, for each stress value,  $\epsilon_{Zn}$  and  $\epsilon_O$  values are easily assigned:

$$\epsilon_{Zn} = \frac{V_{Zn} - V_{Zn,0}}{V_{Zn,0}}, \quad \epsilon_O = \frac{V_O - V_{O,0}}{V_{O,0}}, \quad (13)$$

where the subscript 0 refers to the corresponding equilibrium volume value.

By definition, each  $\sigma_c$  value in Fig. 5 is the same as in the crystal, but the atomic  $\epsilon_c$  is not necessarily equal to the crystal value. Nevertheless, and in concordance with the universal behavior of the  $E$ - $V$  curves [46], we found similar  $\epsilon_c$  values for Zn and O in the three phases. All these results are collected in Table 3. Notice that in this context  $\epsilon_c = \epsilon_{sp}$ . Small differences between atomic critical strengths and the values in the crystal are originated by the fitting procedure.

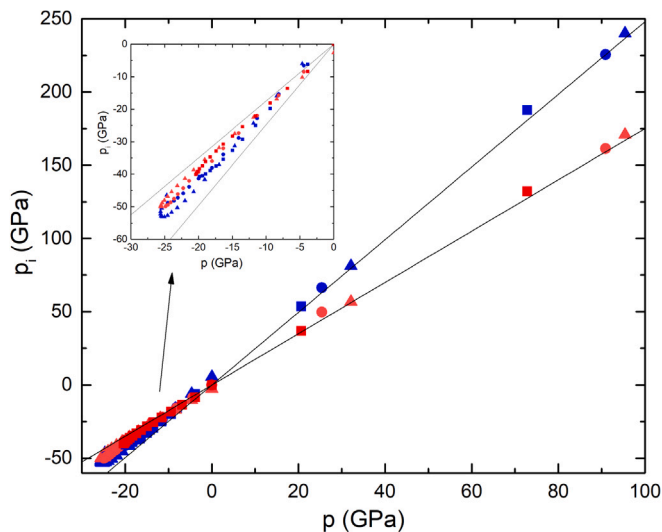


Fig. 6. Calculated  $p$ - $p_i$  curves for Zn (blue), and O (red) for the B1 phase with details (inset) in the negative pressure regime.

When comparing Zn and O results in Table 3 and Fig. 5, we observe that the critical strains of Zn are slightly lower than O. This means that the deformation that the cation can withstand before the crystal rupture is not as large as the one of the oxygen. However, the difference is not noticeable and we can roughly conclude that in these BCSAS crystals, there is not a particular atomic constituent responsible for the crystal instability upon tensile conditions since both, Zn and O, show a similar response in each of the three polymorphs.

To conclude, let us apply the partition of the pressure in terms of atomic mechanical resistances to the spinodal condition. We examine how this decomposition scheme works for negative pressures in Fig. 6. In contrast to the positive pressure regime, we observe a deviation from the linear trend in the  $p$ - $p_i$  plots of the B1, B2, and B3 phases at negative pressures. The cation and the anion consistently tend to equalize their mechanical resistances up to the spinodal point where they become equal and two times higher than the external pressure fulfilling Eq. (5). The fact that the local resistances are equal at the spinodal point suggests that the rupture limit of the material is achieved when all the components of the crystal become unstable. This is an interesting result informing that the atomic mechanical resistances balance each other to produce the rupture of the crystal. Nevertheless, more calculations in other polyatomic crystals are needed to generalize this finding.

## Conclusions

Our investigation was intended to provide a two-fold contribution. We have first emphasized that an accurate computed  $E$ - $V$  curve contains a good description of the mechanical response of a solid not only under pressure but also under “hydrostatic” tensile conditions. We have shown how the common Vinet-EOS [46] can be used to anticipate the critical stress and strain limits of a given material. This opens the possibility of revisiting previously reported  $p$ - $V$  data with the aim of obtaining stability limits of materials at negative pressure. Secondly, our new perspective of the response of a solid to pressure relies on an atomic decomposition with emphasis on the analogy of a crystalline solid as a parallel circuit of atomic mechanical resistors [22,45]. Under this view, it is possible to advance the mechanism by means the solid not only increases its density under pressure but also reaches the rupture point under “hydrostatic” tensile conditions.

In our case study, the atomic partitions reveal that ZnO pressure-induced polymorphs belong to the class of binary crystals with similar atomic sizes (BCSAS). This result has implications for example in

the nucleation and growth process of phase transitions and in the morphology of the new polymorphs. There is not a particular atomic constituent (Zn or O) responding differently to pressure or tensile hydrostatic effects, though Zn is found to be slightly less compressible and to withstand worse negative pressures. We have confirmed that the ZnO crystal and its atomic constituents Zn and O behave more or less the same regardless of which polymorph (B4, B3, B1, and B2) is considered as far as the critical rupture limit is concerned. This result is in concordance with the universal energy-volume relationship. We believe that it is worth exploring if a generalization can be proposed by analyzing other materials with greater complexity than this binary ZnO crystal.

## CRedit authorship contribution statement

**Housseem Lakehal:** Writing – review & editing, Software, Formal analysis, Data curation. **Hocine Chorfi:** Writing – review & editing, Formal analysis, Conceptualization. **Bachir Zouchoune:** Supervision, Funding acquisition, Conceptualization, Writing – review & editing. **Álvaro Lobato:** Conceptualization, Formal analysis, Methodology, Writing – review & editing. **Ruth Franco:** Data curation, Project administration, Supervision, Validation, Writing – original draft. **Pilar Pertierra:** Data curation, Validation, Writing – review & editing. **Miguel Á. Salvadó:** Writing – review & editing, Supervision, Formal analysis, Data curation. **J. Manuel Recio:** Writing – original draft, Project administration, Funding acquisition, Conceptualization.

## Declaration of competing interest

The authors declare that they have no known competing financial interests or personal relationships that could have appeared to influence the work reported in this paper.

## Data availability

Data will be made available on request.

## Acknowledgments

A.L., R.F., P.P., M.A.S., and J.M.R. gratefully acknowledge funding by the Spanish Ministerio de Ciencia e Innovación and Agencia Estatal de Investigación (MCIN/AEI/10.13039/501100011033) as well as the European Regional Development Fund (ERDF, A way of making Europe) through grant PID2021-122585NB-C21(2), and by the Principado de Asturias and the ERDF through grant AYUD/2021/51036. MALTA-Consolider supercomputing center is gratefully acknowledged for its computational facilities. Bachir Zouchoune is grateful to the Algerian DGRSDT (Direction Générale de la Recherche Scientifique et du Développement Technologique) for the financial support.

## References

- [1] Taylor RH, Rose F, Toher C, Levy O, Yang K, Buongiorno Nardelli M, Curtarolo S. A RESTful API for exchanging materials data in the AFLOWLIB.org consortium. *Comput Mater Sci* 2014;93:178–92, URL: <https://doi.org/10.1016/j.commatsci.2014.05.014>.
- [2] Esters M, Oses C, Divilov S, Eckert H, Friedrich R, Hicks D, Mehl MJ, Rose F, Smolyanyuk A, Calzolari A, Campilongo X, Toher C, Curtarolo S. Aflow.org: A web ecosystem of databases, software and tools. *Comput Mater Sci* 2023;216:111808, URL: <https://doi.org/10.1016/j.commatsci.2022.111808>.
- [3] Oses C, Esters M, Hicks D, Divilov S, Eckert H, Friedrich R, Mehl MJ, Smolyanyuk A, Campilongo X, van de Walle A, Schroers J, Kusne AG, Takeuchi I, Zurek E, Buongiorno Nardelli M, Fornari M, Lederer Y, Levy O, Toher C, Curtarolo S. Aflow++: a C++ framework for autonomous materials design. *Comp. Mat. Sci.* 2023;217:111889, URL: <https://doi.org/10.1016/j.commatsci.2022.111889>.
- [4] Merchant A, Batzner S, Schoenholz SS, Aykol M, Cheon G, Cubuk ED. Scaling deep learning for materials discovery. *Nature* 2023;624:80–5, URL: <https://doi.org/10.1038/s41586-023-06735-9>.

- [5] Manjón FJ, Errandonea D, López-Solano J, Rodríguez-Hernández P, Muñoz A. Negative pressures in  $\text{CaWO}_3$  nanocrystals. *J Appl Phys* 2009;105(9):094321, URL: <https://doi.org/10.1063/1.3116727>.
- [6] Lobato A, Recio-Poo M, Otero-de-la Roza A, Salvadó MA, Recio JM. Controlling the off-center positions of anions through thermodynamics and kinetics in flexible perovskite-like materials. *Phys Chem Chem Phys* 2021;23:4491–9, URL: <https://doi.org/10.1039/DOCP05711H>.
- [7] Recio-Poo M, Lobato A, Otero-de-la Roza A, Salvadó MA, Arroyo-de Dompablo ME, Recio JM. Temperature and pressure-induced strains in anhydrous iron trifluoride polymorphs. *Phys Chem Chem Phys* 2021;23:2825–35, URL: <https://doi.org/10.1039/DOCP05888B>.
- [8] Herrero CP, Ramírez R, Herrero-Saboya G. Cubic silicon carbide under tensile pressure: spinodal instability. *Chem Phys* 2023;573:112005, URL: <https://doi.org/10.1016/j.chemphys.2023.112005>.
- [9] Mackenzie AP, Hicks CW. Topological kondo insulators: Negative pressure tuning. *Nature Mater* 2017;16(7):702–3, URL: <https://doi.org/10.1038/nmat4925>.
- [10] Siol S, Holder A, Steffes J, Schelhas LT, Stone KH, Garten L, Perkins JD, Parilla PA, Toney MF, Huey BD, Tumas W, Lany S, Zakutayev A. Negative-pressure polymorphs made by heterostructural alloying. *Sci Adv* 2018;4(4). URL: <http://dx.doi.org/10.1126/sciadv.aag1442>.
- [11] Protesescu L, Yakunin S, Bodnarchuk MI, Krieg F, Caputo R, Hendon CH, Yang RX, Walsh A, Kovalenko MV. Nanocrystals of cesium lead halide perovskites ( $\text{CsPbX}_3$ , X = Cl, Br, and I): Novel optoelectronic materials showing bright emission with wide color gamut. *Nano Lett* 2015;15(6):3692–6, URL: <https://doi.org/10.1021/nl5048779>.
- [12] Chen K, Jin W, Zhang Y, Yang T, Reiss P, Zhong Q, Bach U, Li Q, Wang Y, Zhang H, Bao Q, Liu Y. High efficiency mesoscopic solar cells using  $\text{CsPbI}_3$  perovskite quantum dots enabled by chemical interface engineering. *J Am Chem Soc* 2020;142(8):3775–83, URL: <https://doi.org/10.1021/jacs.9b10700>.
- [13] Gomes EO, Gouveia AF, Gracia L, Lobato A, Recio JM, Andrés J. A chemical-pressure-induced phase transition controlled by lone electron pair activity. *J Phys Chem Lett* 2022;13(42):9883–8, URL: <https://doi.org/10.1021/acs.jpclett.2c02582>.
- [14] Macmillan NH. The ideal strength of solids. In: Latanision RM, Pickeners JR, editors. *Atomistics of fracture*. Boston, MA: Springer US; 1983, p. 95–165.
- [15] Chorfi H, Lobato A, Boudjada F, Salvado MA, Franco R, Baonza VG, Recio JM. Computational modeling of tensile stress effects on the structure and stability of prototypical covalent and layered materials. *Nanomaterials* 2019;9(10):1486, URL: <https://doi.org/10.3390/nano9101483>.
- [16] Bader R. *Atoms in molecules: A quantum theory*. International series of monograph on chemistry. Oxford: Clarendon Press, Oxford University Press; 1990.
- [17] Hazen RM, Finger LW. Bulk modulus—volume relationship for cation-anion polyhedra. *J Geophys Res: Solid Earth* 1979;84(B12):6723–8, URL: <https://doi.org/10.1029/JB084iB12p06723>.
- [18] Finger LW, Hazen RM, Hofmeister AM. High-Pressure crystal chemistry of spinel ( $\text{MgAl}_2\text{O}_4$ ) and magnetite ( $\text{Fe}_3\text{O}_4$ ): Comparisons with silicate spinels. *Phys Chem Miner* 1986;13(4):215–20, URL: <https://doi.org/10.1007/BF00308271>.
- [19] Recio JM, Franco R, Martín Pendás A, Blanco MA, Pueyo L, Pandey R. Theoretical explanation of the uniform compressibility behavior observed in oxide spinels. *Phys Rev B* 2001;63:184101, URL: <https://doi.org/10.1103/PhysRevB.63.184101>.
- [20] Vidal-Daza I, Sanchez-Navas A, Hernandez-Laguna A. Compressional behavior of the aragonite-structure carbonates to 6 GPa. *Phys Chem Miner* 2023;50(2). URL: <https://doi.org/10.1007/s00269-023-01237-6>.
- [21] Martín Pendás A, Costales A, Blanco MA, Recio JM, Luaña V. Local compressibilities in crystals. *Phys Rev B* 2000;62:13970–8, URL: <https://doi.org/10.1103/PhysRevB.62.13970>.
- [22] Ouahrani T, Menendez JM, Marqués M, Contreras-García J, Baonza VG, Recio JM. Local pressures in Zn chalcogenide polymorphs. *Europhys Lett* 2012;98(5):56002, URL: <http://dx.doi.org/10.1209/0295-5075/98/56002>.
- [23] Gonze X, Amadon B, Anglade P-M, Beuken J-M, Bottin F, Boulanger P, Bruneval F, Caliste D, Caracas R, Côté M, Deutsch T, Genovese L, Ghosez P, Giantomassi M, Goedecker S, Hamann D, Hermet P, Jollet F, Jomard G, Leroux S, Mancini M, Mazevet S, Oliveira M, Onida G, Pouillon Y, Rangel T, Rignanese G-M, Sangalli D, Shaltaf R, Torrent M, Verstraete M, Zerah G, Zwanziger J. ABINIT: First-principles approach to material and nanosystem properties. *Comput Phys Comm* 2009;180(12):2582–615, URL: <https://doi.org/10.1016/j.cpc.2009.07.007>.
- [24] Perdew JP, Burke K, Ernzerhof M. Generalized gradient approximation made simple. *Phys Rev Lett* 1996;77:3865–8, URL: <https://doi.org/10.1103/PhysRevLett.77.3865>.
- [25] Troullier N, Martins JL. Efficient pseudopotentials for plane-wave calculations. *Phys Rev B* 1991;43(3):1993–2006, URL: <https://doi.org/10.1103/PhysRevB.43.1993>.
- [26] Monkhorst HJ, Pack JD. Special points for brillouin-zone integrations. *Phys Rev B* 1976;13:5188–92, URL: <https://doi.org/10.1103/PhysRevB.13.5188>.
- [27] Head JD, Zerner MC. A Broyden—Fletcher—Goldfarb—Shanno optimization procedure for molecular geometries. *Chem Phys Lett* 1985;122(3):264–70, URL: [https://doi.org/10.1016/0009-2614\(85\)80574-1](https://doi.org/10.1016/0009-2614(85)80574-1).
- [28] Momma K, Izumi F. VESTA3 for three-dimensional visualization of crystal, volumetric and morphology data. *J Appl Crystallogr* 2011;44(6):1272–6, URL: <https://doi.org/10.1107/S0021889811038990>.
- [29] Blanco M, Francisco E, Luaña V. GIBBS: isothermal-isobaric thermodynamics of solids from energy curves using a quasi-harmonic Debye model. *Comput Phys Comm* 2004;158(1):57–72, URL: <https://doi.org/10.1016/j.comphys.2003.12.001>.
- [30] Otero-de-la Roza A, Abbasi-Pérez D, Luaña V. Wałkowska A. X-ray diffraction at high pressure and high or low temperature using synchrotron radiation: Selected applications in studies of spinel structures. *J Alloys Compd* 2005;401(1):11–7, URL: <https://doi.org/10.1016/j.jallcom.2005.01.107>.
- [31] Flórez M, Contreras-García J, Recio JM, Marqués M. Quantum-mechanical calculations of zircon to scheelite transition pathways in  $\text{ZrSiO}_4$ . *Phys Rev B* 2009;79:104101, URL: <https://link.aps.org/doi/10.1103/PhysRevB.79.104101>.
- [32] Salvadó MA, Franco R, Pertierra P, Ouahrani T, Recio JM. Hysteresis and bonding reconstruction in the pressure-induced B3–B1 phase transition of 3 C-SiC. *Phys Chem Chem Phys* 2017;19:22887–94, URL: <https://doi.org/10.1039/C7CP03732E>.
- [33] Wang B, Wang H, Tu B, Xu P, Wang W, Fu Z. Theoretical insight into optical properties of  $\text{ZnGa}_2\text{O}_4$  transparent ceramic. *Mater Today Commun* 2023;34:104846, URL: <https://doi.org/10.1016/j.mtcomm.2022.104846>.
- [34] Recio JM, Blanco MA, Luaña V, Pandey R, Gerward L, Staun Olsen J. Compressibility of the high-pressure rocksalt phase of ZnO. *Phys Rev B* 1998;58:8949–54, URL: <https://doi.org/10.1103/PhysRevB.58.8949>.
- [35] Maouche D, Saoud FS, Louail L. Dependence of structural properties of ZnO on high pressure. *Mater Chem Phys* 2007;106(1):11–5, URL: <https://doi.org/10.1016/j.matchemphys.2007.05.029>.
- [36] Kurkcu C, Merdan Z, Yamicier C. Pressure-induced phase transitions, electronic, elastic and vibrational properties of zinc oxide under high pressure. *Indian J Phys* 2019;93(8):979–89, URL: <https://doi.org/10.1007/s12648-018-01365-8>.
- [37] Wang X-W, Sun X-W, Song T, Tian J-H, Liu Z-J. 2022.
- [38] Desgreniers S. High-density phases of ZnO: Structural and compressive parameters. *Phys Rev B* 1998;58:14102–5. <http://dx.doi.org/10.1103/PhysRevB.58.14102>, URL: <https://link.aps.org/doi/10.1103/PhysRevB.58.14102>.
- [39] Recio JM, Pendás AM, Francisco E, Flórez M, Luaña V. Low- and high-pressure ab initio equations of state for the alkali chlorides. *Phys Rev B* 1993;48:5891–901, URL: <https://doi.org/10.1103/PhysRevB.48.5891>.
- [40] Hofmeister AM. IR spectroscopy of alkali halides at very high pressures: Calculation of equations of state and of the response of bulk moduli to the B1-B2 phase transition. *Phys Rev B* 1997;56:5835–55, URL: <https://doi.org/10.1103/PhysRevB.56.5835>.
- [41] Shannon RD. Revised effective ionic radii and systematic studies of interatomic distances in halides and chalcogenides. *Acta Crystallogr Sect A* 1976;32(5):751–67, URL: <https://doi.org/10.1107/S0567739476001551>.
- [42] Zahn D, Leoni S. Mechanisms and nucleation characteristics of the pressure-induced B1–B2 transition in potassium halides: A question of ion hardness and softness. *J Phys Chem B* 2006;110(22):10873–7, URL: <https://doi.org/10.1021/jp061538f>.
- [43] Ouahrani T, Franco R, Menéndez J, Marqués M, Recio J. Microscopic partition of pressure and elastic constants in CdTe polymorphs. *J Alloys Compd* 2014;592:150–6, URL: <https://doi.org/10.1016/j.jallcom.2013.12.153>.
- [44] Vinet P, Rose J, Ferrante J, Smith J. Universal features of the equation of state of solids. *J Phys Condens Matter* 1989;1(11):1941–63, URL: <http://dx.doi.org/10.1088/0953-8984/1/11/002>.
- [45] Brosh E, Makov G, Shneck RZ. The spinodal constraint on the equation of state of expanded fluids. *J Phys: Condens Matter* 2003;15(19):2991, URL: <http://dx.doi.org/10.1088/0953-8984/15/19/303>.
- [46] Lobato A, Salvadó MA, Recio JM, Taravillo M, Baonza VG. Highs and lows of bond lengths: is there any limit? *Angew Chem Int Edn* 2021;60(31):17028–36, URL: <https://doi.org/10.1002/anie.202102967>.